Oligodendrocyte dependent synchronized activity orchestrates circuit maturation and brain functionalization

Authors: Ryo Masumura[1], Kyosuke Goda[1], Mariko Sekiguchi[1], Naofumi Uesaka[1]*

Affiliations:

[1]Department of Cognitive Neurobiology, Graduate School of Medical and Dental Sciences, Tokyo Medical and Dental University (TMDU), Tokyo 113-8510, Japan.

*Corresponding author.

Naofumi Uesaka[1]*

[1] Department of Cognitive Neurobiology, Graduate School of Medical and Dental Sciences, Tokyo Medical and Dental University (TMDU), Tokyo 113-8510, Japan.

*Corresponding author. Email: uesaka.cnb@tmd.ac.jp

Abstract:

Immature animals have the ability to interact with their environment, indicating that complex neural circuits are formed through mechanisms of self-organization. Correlated spontaneous activity among neurons suggests a universal principle behind the self-organization of complex neural circuits(1, 2), though the underlying mechanisms and functional roles in the central nervous system remain unclear. Here, we show that oligodendrocyte-dependent synchronized spontaneous activity during the critical period is indispensable for neural circuit refinement and brain functionalization. We found that oligodendrocyte deletion during specific time window disrupts Purkinje cell activity synchrony and synapse elimination in the mouse cerebellum. We further demonstrated that synchronized spontaneous activity is a prerequisite for synapse elimination. Behavioral analyses linked these developmental disruptions to adult cerebellar function, manifesting as anxiety-like behavior, reduced social interaction, and compromised motor coordination in adult mice. This association indicates the significance of following the appropriate developmental trajectory to ensure the integrity of brain function, suggesting that oligodendrocytes during development are vital organizers of brain functionalization. Our findings highlight the crucial role of oligodendrocytes in orchestrating synapse elimination and optimizing brain function through the mediation of synchronized activity during specific developmental stages.

Main Text

The ability of immature animals to respond to environmental stimuli and produce various outputs even before the onset of sensory inputs suggests that complex neural networks are pre-organized, supported by strong developmental processes. A key process is spontaneous activity, which emerges as a fundamental driver shaping neural circuits through mechanisms that remain only partially understood. Spontaneous activity is highly correlated in neural populations during early postnatal development across various species and neural systems (1, 2). The widespread occurrence of the correlated spontaneous activity suggests a fundamental and universal principle driving brain maturation, where the activity may facilitate the establishment of precise sensory maps and extensive neural networks required for sensory information processing and outputs. Despite its recognized importance, the mechanisms underlying the correlated spontaneous activity in the central nervous system and its role in brain maturation, particularly in relation to brain functionalization, remain unclear.

In the developing central nervous system, correlated spontaneous activity begins as synchronized patterns in localized or extensive areas (3-8). Synchronized patterns then transition to desynchronized states as seen in the cortex, cerebellum, and olfactory bulb(3, 7, 8). The maturation of excitatory and inhibitory synapses, synapse elimination, local network dynamics, and inputs from other regions have been suggested as candidate mechanisms that cause synchronized spontaneous activity and mediate the transition from the synchronization to desynchronization. However, the involvement of glial cells has not been explored. Oligodendrocytes, one type of glial cells, are traditionally known for their role in myelination and regulation of conduction velocity. Emerging studies indicate that oligodendrocytes might also contribute to neural activity synchronization and brain function in the adult animals (9-11). However, roles of oligodendrocytes in the developing brain remain largely unknown. Our research aims to elucidate the mechanisms underlying synchronized spontaneous activity in the developing mouse cerebellum, with a focus on oligodendrocytes, and explore the roles of oligodendrocyte-mediated synchronized spontaneous activity in the context of neural circuit maturation and brain functionalization.

Developmental oligodendrocytes regulate synchronized spontaneous activity

To elucidate the role of oligodendrocytes in the regulation of synchronized spontaneous activity, we engineered an oligodendrocyte-specific adeno-associated virus (OL-AAV) characterized by a human myelin associated glycoprotein (hMAG) promoter and an oligodendrocyte directional capsid, and employed it for a genetic approach to developmental oligodendrocytes (Fig. 1a). We focused on the developing mouse cerebellum in which synchronized spontaneous activity and synapse elimination were observed during postnatal development (7, 12). Mature oligodendrocytes and myelination appeared in the cerebellum during postnatal day 5 (P5) to P7 (Extended Data Fig. 1a-b). Injection of OL-AAVs expressing mCherry into the cerebellum of P7 mice resulted in selective expression of mCherry in cerebellar oligodendrocytes at P21 (>98%) (Fig. 1b-d). Injection of OL-AAVs expressing Diphtheria toxin A (DTA) into the cerebellum of postnatal day 7 (P7) mice resulted in a significant reduction of oligodendrocytes and myelination by P10 and P14, with the recovery of the number of oligodendrocytes and the extent of myelination observed by P21 and in adulthood (Fig. 1e-f and Extended Data Fig. 1c-d). This temporal pattern of oligodendrocyte deletion allowed us to specifically assess the role of these cells during a critical window of cerebellar development.

We tested whether oligodendrocyte deficit affected synchronized spontaneous activity in the cerebellar Purkinje cell (PC) population. PCs show synchronized spontaneous activity in response to climbing fiber synaptic inputs in newborn mice and exhibit progressive desynchronization as development progresses (7). In vivo calcium imaging of PCs revealed a marked reduction in synchrony of spontaneous activity among PCs at P13-15 following oligodendrocyte deletion (Fig. 1g-h and Extended Data Fig. 2a-b). This effect was observed across both proximal and distal PC populations (Fig. 1i and Extended Data Fig. 2c), indicating a widespread disruption of neural activity synchronization. Notably, other parameters such as frequency, amplitude, and area of calcium transients remained unchanged (Fig. 1j-l), suggesting a specific effect on PC activity synchrony rather than general neural activity.

Developmental oligodendrocytes regulate synapse elimination

During the second and third postnatal week, the developing cerebellar circuit undergoes significant maturation, one aspect of which is the synapse elimination of climbing fiber to PC projection (CF-PC) (12, 13). Synapse elimination, characterized by the strengthening

of some synapses and the weakening and subsequent elimination of others, is thought to be involved in the transition of synchronized spontaneous activity and play a critical role in brain functionallization (7, 14). To examine roles of oligodendrocytes in CF synapse elimination, we injected OL-AAVs with DTA into the mouse cerebellum at P7 and analyzed CF-PC synapse elimination by electrophysiological and histochemical methods (15, 16). We found that oligodendrocyte deletion caused a significant increase in the number of CFs innervating each PC without changes in total CF-EPSC amplitude, paired-pulse ratio, or disparity ratio at P21-P28 (Fig. 2 a-c and Extended Data Fig. 3a-b). Additionally, the number of CF terminals on PC somata was notably larger in oligodendrocyte-deficient mice than that of PC somata in the control mice (Fig. 2d-e). In oligodendrocyte-deficient mice, the height of CF innervation on PC dendrites was apparently reduced compared with control mice (Fig. 2f-g). These results indicate that oligodendrocyte deletion leads to impaired elimination of CF synapses from PC somata and disturbed full innervation of CFs on PC dendrites.

We examined whether these effects of oligodendrocyte deletion could be attributed to changes in synaptic inputs from inhibitory neurons and parallel fibers (PFs) to PCs which greatly influence CF synapse elimination (17-19) and those changes may modulate synchronized spontaneous activity of PC population. The amplitude and frequency of miniature inhibitory postsynaptic currents (mIPSCs) were not different between control and oligodendrocyte-deficient mice (Extended Data Fig. 3c-e). Relationships between the amplitude of PF-mediated EPSC and the strength of PF stimulus were similar between control and oligodendrocyte-deficient mice (Extended Data Fig. 3f-g). We also analyzed other glial cells, Bergmann glia and microglia which have been shown to affect CF synapse elimination (20, 21). The density and the immunostaining pattern of Bergmann glia and microglia were not altered in oligodendrocyte-deficient cerebellum (Extended Data Fig. 3h-k). Our findings suggest that the observed disruptions in PC activity synchrony and CF synapse elimination are not indirectly caused by alterations in PF-PC synapses, inhibitory synaptic inputs, or other glial cells such as astrocyte and microglia.

Synchronized spontaneous activity promotes synapse elimination

Building on the findings that oligodendrocytes play a pivotal role in maintaining synchronized spontaneous activity and organizing synapse elimination in the developing cerebellum, we next tested the possibility that synchronized spontaneous activity regulates synapse elimination. Our experiments were designed to dissect the temporal

sequence and causal relationship between these two processes. Initial analyses focused on determining the sequence of events following oligodendrocyte deletion by the injection of OL-AAVs DTA at P7. At P10-P11, oligodendrocyte-deficient mice exhibited a significant reduction in PC activity synchrony without alterations in other neural activity parameters (Extended Data Fig. 4). In contrast, at this developmental stage, CF synapse elimination remained unaffected by the loss of oligodendrocytes (Extended Data Fig. 5a-b). The ablation of oligodendrocytes was found not to influence the total CF−EPSC amplitude and disparity ratio during the P10-P11 (Extended Data Fig. 5c-d). PPR was found to be elevated by oligodendrocyte ablation (Extended Data Figure 5e), indicating alterations in the properties of CFs. We further found that the EPSC amplitude of weaker CFs, which were shown to remain on PC somata and eventually eliminated, was significantly larger in oligodendrocyte-deficient mice than control mice (Extended Data Fig. 5f). The EPSC amplitude of strongest CFs, which were shown to translocate into PC dendrites, was not different between control and DTA (Extended Data Fig. 5g). These findings collectively suggest that the disruption of synchronized spontaneous activity precedes abnormalities in synapse elimination, which may be mediated through the impairment of activity-dependent synaptic plasticity (see discussion) (22, 23).

To directly test the causal link between synchronized spontaneous activity and synapse elimination, we employed a novel experimental strategy involving the selective manipulation of CF activity which induces PC calcium transients. We manipulated the synchronized spontaneous activity of PC population through the expression of Kir2.1, a potassium channel known to reduce neuronal excitability, in a subset of CFs whose synaptic inputs induce calcium transients in PCs (7, 24). The co-injection of AAVs with EGFP or Kir2.1-T2A-GFP under the control of TRE promoter and AAVs with tetracycline transactivator (tTA) under the control of Htr5b promoter (25) into the mouse inferior olivary nucleus at P7 resulted in a subset of CFs being labeled with EGFP in the cerebellum at P22 (Extended Data Fig. 6a-c). We confirmed by in vivo calcium imaging of CFs that activity of CFs with Kir2.1-T2A-jGCaMP7 was lower than that for CFs with only jGCaMP7 at P13-15 (Extended Data Fig. 6d-g). In vivo calcium imaging of PC population revealed that the synchrony of spontaneous activity of PC population with a subset of CFs which expressed Kir2.1 was lower than that for control mice at P13-15 (Fig. 3a-c and Extended Data Fig. 6h-i). The frequency and area of calcium transients were not altered by Kir2.1 expression in a subset of CFs (Extended Data Fig. 6j and 6l). The amplitude of calcium transients tended to be lower in Kir2.1 expressing mice than that for control mice ($p = 0.065$, Extended Data Fig. 6k). These results indicate that kir2.1 expression in a subset of CFs leads to reduced synchrony of PC population activity.

We examined the effects of altered synchrony of PC population activity on CF synapse elimination and found that the reduction of the synchrony of PC population activity resulted in a marked impairment in CF synapse elimination, as evidenced by the increased number of CF terminals on PC somata (Fig. 3d-f). Moreover, the height of CF innervation on PC dendrites in these mice with kir2.1 in a subset of CFs was apparently reduced compared with control mice (Fig. 3d-e and h-i). These effects were not limited to PCs whose dendrites were directly innervated by Kir2.1-expressing CFs but also extended to neighboring PC (Fig. 3g and i), suggesting that reduced synchrony impairs synapse elimination, not necessarily by the effect of reduced CF activity itself. These data indicate the critical role of synchronized spontaneous activity in guiding synapse elimination.

Developmental oligodendrocyte affects brain function via synchronized spontaneous activity and synapse elimination

We explored whether oligodendrocyte during cerebellar development modulates adult brain function. We have discovered that selective oligodendrocyte ablation in the cerebellum during early postnatal development results in persistent hyposynchrony of PC activity into adulthood, while leaving other PC activity parameters unchanged (Extended Data Fig. 7), raising the possibility that oligodendrocyte deletion during development affects brain function. We investigated the role of developmental oligodendrocytes in modulating cerebellar function. We injected OL-AAVs with hMAG-mCherry or hMAG-DTA at P6-7 into distinct compartments (left, center, right) of the cerebellum (Extended Data Fig. 8), aligning with the cerebellum's functional segmentation (26, 27) and investigated several brain function including activity, anxiety like behavior, sociality, and motor function at adult stages. Behavioral assessments in adulthood unveiled that oligodendrocyte deletion in the cerebellum during development precipitates anxiety-like behavior specifically when targeted to the central cerebellar region, but did not affect distance travelled, underscoring the compartment-specific role in anxiety regulation (Fig. 4a-c). Additionally, across all regions, mice with oligodendrocyte deletion during development exhibited diminished sociality and impaired motor coordination, evidenced by reduced social approach to novel mouse and decreased latency to fall in the Rotarod test, respectively (Fig. 4d-g).

We next examined a critical period for oligodendrocyte influence on cerebellar function and a link between synapse elimination and cerebellar function. We administrated hMAG-DTA to the central cerebellum at postnatal week 3 (3W_DTA

mice), when synaptic elimination is completed. Oligodendrocytes in the cerebellum of mice injected by hMAG-DTA were significantly reduced at 4 weeks (1 week after AAV injection) compared with control mice with only hMAG-mCherry, but were returned to the number similar to control mice at 2 months old (Extended Data Fig. 9a-c), indicating a temporary effect of the ablation. Oligodendrocyte deletion after synaptic elimination process did not alter CF synapse configuration on PCs (Extended Data Fig. 9d-e), suggesting that oligodendrocytes after 3 weeks old are not involved in CF synapses. Calcium imaging analysis of 3W_DTA mice at 4weeks old revealed the reduction in the amplitude and area of PC calcium transients, but not in frequency and correlation coefficient (Extended Data Fig. 10). This data suggest that oligodendrocytes play distinct roles in PC activity before and after the synapse elimination process in the cerebellum. Behavioral assessments in adulthood of these mice uncovered no significant behavioral anomalies in anxiety or sociality (Extended Data Fig. 11a-e). However, the mice injected by hMAG-DTA showed a deficit in motor learning or peak performance as evidenced by diminished performance at day3 in the Rotarod test (Extended Data Fig. 11f). These data suggest that oligodendrocytes during the specific window in development regulate the subsequent behaviors and that synapse elimination may contribute to functional integrity of sociality and mentality.

To clarify a link between synchronized PC activity during developmental stage and cerebellar function, we analyzed behaviors at 2 months old for mice expressing Kir2.1 in a subset of CFs from developmental stage (Fig. 3 and Extended Data Fig. 6, injection of AAVs with Kir2.1 at P7). We found that the impaired synchronization of PC population activity in the cerebellum from developmental stages lead to diminished sociality and impaired motor coordination, evidenced by reduced social approach to novel mouse and decreased latency to fall in the Rotarod test, respectively. Distance travelled and percentage time spent in center in kir2.1-expressing mice tented to decrease compared with those for control, though not statistically significant (Fig. 4h-m). Those results indicate that the behavioral consequences of ablating oligodendrocytes during development are similar to those of reducing synchrony during development. Together, our comprehensive analyses reveal a pivotal role for oligodendrocytes during developmental critical periods, affecting cerebellar functionalization through mechanisms involving both synchronized spontaneous activity and synaptic elimination.

Discussion

This study provides compelling evidence that oligodendrocytes play a crucial role beyond their traditional functions in myelination, extending to the regulation of synchronized spontaneous activity and synapse elimination, and emphasizing the complexity of glial-neuronal interactions in the developing brain. Moreover, our research illuminates the significance of brain development following a proper course in brain function integrity

In adult brain, adaptive myelination can induce and maintains synchrony of spontaneous activity among neural populations (9, 11, 28). Developmental oligodendrocytes have been also speculated to regulate the synchrony of neuronal activities (29) . Our present study directly demonstrate that developmental oligodendrocytes regulate the synchrony of neuronal spontaneous activity. Myelin formation and plasticity modulates axonal conduction velocity, while signals from neurons are known to induce myelination (30). The modulation of axonal conduction velocity through oligodendrocyte-neuron interactions may result in synchrony of spontaneous activity among neuronal populations during development, and changes in these interactions may cause desynchronization.

Oligodendrocytes and oligodendrocyte precursor cells (OPCs) have functions for synapses that are only gradually understood (31, 32). Recently, OPCs have been shown to be involved in synapse elimination (33, 34). To our knowledge, our data provides the first evidence that oligodendrocytes regulate synapse elimination. We further reveal that synchronized spontaneous activity mediates the regulation of synapse elimination by oligodendrocytes. A plausible mechanism is that synaptic plasticity induced by synchronized spontaneous activity strengthens some synapses and fibers, and eliminate other then. It has been shown that spike timing dependent plasticity and synaptic amplitude dependent plasticity of CF-PC synapses in the developing cerebellum can be involved in CF synapse elimination (22, 23). A protocol, consisting of the pairing of CF activity with spike activity in the postsynaptic PC, results in LTP for CFs with large synaptic inputs, which are eventually strengthened/maintained, and LTD for them with small synaptic inputs. Since temporally clustered multiple CF inputs induce activity and calcium transients in PCs during development (23), synchronized spontaneous activity among CFs controlled by oligodendrocytes can underlie such plasticity dependent synapse elimination.

Correlated spontaneous activity have been shown to play a pivotal role in neural development and the establishment of functional neural circuits especially in the developing visual system (1, 2). Retinal waves observed in various species, play a fundamental role in developing interconnections within the visual system including

topographic maps. Recent study demonstrates that retinal wave not merely random but possesses an intrinsic directionality that prefigures the optic flow patterns encountered after eye opening. However, the effects of correlated spontaneous activity during development on brain functionalization remain largely unknown. Our study suggests that synchronized spontaneous activity during development play a crucial role in the subsequent brain functionalization, probably through the mediation of synapse elimination. These studies provide new insights into specific information content carried by correlated spontaneous activity and their influence on the development of brain functions including higher-order function, extending beyond the previously understood role of these activity in neural circuit maturation.

There is growing evidence that oligodendrocytes and myelin affect learning, memory, and cognitive function (35, 36). Moreover, numerous studies have reported the changes of white matter, oligodendrocyte, and myelin in schizophrenia, autism spectrum disorders, depression, and anxiety, suggesting that the deficit of oligodendrocytes and myelin may underlie multiple brain disorders (35, 37). However, it is unclear when, where, and how oligodendrocytes and myelin are involved in the functionalization of brain and the pathogenesis of these brain disorders. Past studies suggest that synapse elimination deficit is one of the etiologies of multiple brain diseases (14). Our data that synchronized spontaneous activity during development controlled by oligodendrocytes is a precursor to effective synapse elimination—and, by extension, to the maturation of functional neural circuits and brain functions—provides a novel lens through which to examine the etiology of disorders characterized by synaptic imbalances and dysregulation of neural activity. Thus, oligodendrocyte and myelination abnormalities, and the resulting disruption of correlated activity and synapse elimination in neuronal populations, may be new therapeutic targets for multiple brain disorders.

Given the pivotal role of oligodendrocytes in neural circuit maturation, future research should aim to further dissect the molecular and cellular mechanisms underpinning their influence on synchronized spontaneous activity and synapse elimination. Understanding the signaling pathways and interaction networks involved could open new therapeutic avenues for addressing developmental brain disorders and enhancing neural repair after injury.

Acknowledgments: We thank Dr. Daisuke Tanaka, Dr. Shizuki Inaba, Dr. Ayaka Nakai, and other lab members of Uesaka lab for helpful comments and discussions.

Funding: This work is supported by MEXT Grants-in-Aid for Scientific Research on transformative research area B "Design-build of brain through spontaneous brain multimodal activity" (KAKENHI 22H05092, 22H05093), the Asahi Glass Foundation, Toray Foundation, Takeda Science Foundation, Tokumori Yasumoto Memorial Trust, and Uehara Memorial Foundation to N.U.

Author contributions: Initiation and conceptualization: N.U. Investigation: R.M., K.G., M.S., and N.U. Writing - original draft: N.U. Writing - editing: R.M., K.G., N.U., with inputs from all authors. Visualization: R.M., and N.U. Supervision: N.U. Funding acquisition: N.U.

Competing interests: The authors declare no conflicts of interest.

Data and materials availability: All data are available in the main text or the supplementary materials.

References:

1 Ackman, J. B. & Crair, M. C. Role of emergent neural activity in visual map development. *Current opinion in neurobiology* **24**, 166-175, doi:10.1016/j.conb.2013.11.011 (2014).

2 Kirkby, L. A., Sack, G. S., Firl, A. & Feller, M. B. A role for correlated spontaneous activity in the assembly of neural circuits. *Neuron* **80**, 1129-1144, doi:10.1016/j.neuron.2013.10.030 (2013).

3 Fujimoto, S. *et al.* Activity-dependent local protection and lateral inhibition control synaptic competition in developing mitral cells in mice. *Dev Cell* **58**, 1221-1236 e1227, doi:10.1016/j.devcel.2023.05.004 (2023).

4 Babola, T. A. *et al.* Homeostatic Control of Spontaneous Activity in the Developing Auditory System. *Neuron* **99**, 511-524 e515, doi:10.1016/j.neuron.2018.07.004 (2018).

5 Adelsberger, H., Garaschuk, O. & Konnerth, A. Cortical calcium waves in resting newborn mice. *Nat Neurosci* **8**, 988-990, doi:10.1038/nn1502 (2005).

6 Murakami, T., Matsui, T., Uemura, M. & Ohki, K. Modular strategy for development of the hierarchical visual network in mice. *Nature* **608**, 578-585, doi:10.1038/s41586-022-05045-w (2022).

7 Good, J. M. *et al.* Maturation of Cerebellar Purkinje Cell Population Activity during Postnatal Refinement of Climbing Fiber Network. *Cell Rep* **21**, 2066-2073, doi:10.1016/j.celrep.2017.10.101 (2017).

8 Mizuno, H. *et al.* Patchwork-Type Spontaneous Activity in Neonatal Barrel Cortex Layer 4 Transmitted via Thalamocortical Projections. *Cell Rep* **22**, 123-135, doi:10.1016/j.celrep.2017.12.012 (2018).

9 Kato, D. *et al.* Motor learning requires myelination to reduce asynchrony and spontaneity in neural activity. *Glia* **68**, 193-210, doi:10.1002/glia.23713 (2020).

10 Pajevic, S., Basser, P. J. & Fields, R. D. Role of myelin plasticity in oscillations and synchrony of neuronal activity. *Neuroscience* **276**, 135-147, doi:10.1016/j.neuroscience.2013.11.007 (2014).

11 Pajevic, S., Plenz, D., Basser, P. J. & Fields, R. D. Oligodendrocyte-mediated myelin plasticity and its role in neural synchronization. *Elife* **12**, doi:10.7554/eLife.81982 (2023).

12 Kano, M., Watanabe, T., Uesaka, N. & Watanabe, M. Multiple Phases of Climbing Fiber Synapse Elimination in the Developing Cerebellum. *Cerebellum* **17**, 722-734, doi:10.1007/s12311-018-0964-z (2018).

13 Kano, M. & Watanabe, T. Developmental synapse remodeling in the cerebellum and visual thalamus. *F1000Res* **8**, doi:10.12688/f1000research.18903.1 (2019).

14 Penzes, P., Cahill, M. E., Jones, K. A., VanLeeuwen, J. E. & Woolfrey, K. M. Dendritic spine pathology in neuropsychiatric disorders. *Nat Neurosci* **14**, 285-293, doi:10.1038/nn.2741 (2011).

15 Kano, M. *et al.* Impaired synapse elimination during cerebellar development in PKCγ mutant mice. *Cell* **83**, 1223-1231, doi:0092-8674(95)90147-7 [pii] (1995).

16 Uesaka, N. *et al.* Retrograde semaphorin signaling regulates synapse elimination in the developing mouse brain. *Science* **344**, 1020-1023, doi:10.1126/science.1252514 (2014).

17 Hashimoto, K. *et al.* Roles of glutamate receptor δ2 subunit (GluRδ2) and metabotropic glutamate receptor subtype 1 (mGluR1) in climbing fiber synapse elimination during postnatal cerebellar development. *J Neurosci* **21**, 9701-9712, doi:21/24/9701 [pii] (2001).

18 Kurihara, H. *et al.* Impaired parallel fiber-->Purkinje cell synapse stabilization during cerebellar development of mutant mice lacking the glutamate receptor δ2 subunit. *J Neurosci* **17**, 9613-9623 (1997).

19 Nakayama, H. *et al.* GABAergic inhibition regulates developmental synapse elimination in the cerebellum. *Neuron* **74**, 384-396, doi:10.1016/j.neuron.2012.02.032 (2012).

20 Miyazaki, T. *et al.* Glutamate transporter GLAST controls synaptic wrapping by Bergmann glia and ensures proper wiring of Purkinje cells. *Proc Natl Acad Sci U S A* **114**, 7438-7443, doi:10.1073/pnas.1617330114 (2017).

21 Nakayama, H. *et al.* Microglia permit climbing fiber elimination by promoting GABAergic inhibition in the developing cerebellum. *Nat Commun* **9**, 2830, doi:10.1038/s41467-018-05100-z (2018).

22 Bosman, L. W., Takechi, H., Hartmann, J., Eilers, J. & Konnerth, A. Homosynaptic long-term synaptic potentiation of the "winner" climbing fiber synapse in developing Purkinje cells. *J Neurosci* **28**, 798-807, doi:28/4/798 [pii] 10.1523/JNEUROSCI.4074-07.2008 (2008).

23 Kawamura, Y. *et al.* Spike timing-dependent selective strengthening of single climbing fibre inputs to Purkinje cells during cerebellar development. *Nat Commun* **4**, 2732, doi:10.1038/ncomms3732 (2013).

24 Hashimoto, K. *et al.* Postsynaptic P/Q-type Ca2+ channel in Purkinje cell mediates synaptic competition and elimination in developing cerebellum. *Proc Natl Acad Sci U S A* **108**, 9987-9992, doi:10.1073/pnas.1101488108 (2011).

25 Dorgans, K., Guo, D., Kurima, K., Wickens, J. & Uusisaari, M. Y. Designing AAV Vectors for Monitoring the Subtle Calcium Fluctuations of Inferior Olive Network in vivo. *Front Cell Neurosci* **16**, 825056, doi:10.3389/fncel.2022.825056 (2022).

26 Guell, X., Schmahmann, J. D., Gabrieli, J. & Ghosh, S. S. Functional gradients of the cerebellum. *Elife* **7**, doi:10.7554/eLife.36652 (2018).

27 Manni, E. & Petrosini, L. A century of cerebellar somatotopy: a debated representation. *Nature reviews. Neuroscience* **5**, 241-249, doi:10.1038/nrn1347 (2004).

28 Bonetto, G., Belin, D. & Karadottir, R. T. Myelin: A gatekeeper of activity-dependent circuit plasticity? *Science* **374**, eaba6905, doi:10.1126/science.aba6905 (2021).

29 Jang, M., Gould, E., Xu, J., Kim, E. J. & Kim, J. H. Oligodendrocytes regulate presynaptic properties and neurotransmission through BDNF signaling in the mouse brainstem. *Elife* **8**, doi:10.7554/eLife.42156 (2019).

30 Fields, R. D. A new mechanism of nervous system plasticity: activity-dependent myelination. *Nature reviews. Neuroscience* **16**, 756-767, doi:10.1038/nrn4023 (2015).

31 Liu, Y. *et al.* Interactions of glial cells with neuronal synapses, from astrocytes to microglia and oligodendrocyte lineage cells. *Glia* **71**, 1383-1401, doi:10.1002/glia.24343 (2023).

32 Wilton, D. K., Dissing-Olesen, L. & Stevens, B. Neuron-Glia Signaling in Synapse Elimination. *Annu Rev Neurosci* **42**, 107-127, doi:10.1146/annurev-neuro-070918-050306 (2019).

33 Auguste, Y. S. S. *et al.* Oligodendrocyte precursor cells engulf synapses during circuit remodeling in mice. *Nat Neurosci* **25**, 1273-1278, doi:10.1038/s41593-022-01170-x (2022).

34 Yamazaki, Y. *et al.* Region- and Cell Type-Specific Facilitation of Synaptic Function at Destination Synapses Induced by Oligodendrocyte Depolarization. *J Neurosci* **39**, 4036-4050, doi:10.1523/JNEUROSCI.1619-18.2019 (2019).

35 de Faria, O., Jr. *et al.* Periods of synchronized myelin changes shape brain function and plasticity. *Nat Neurosci* **24**, 1508-1521, doi:10.1038/s41593-021-00917-2 (2021).

36 Munyeshyaka, M. & Fields, R. D. Oligodendroglia are emerging players in several forms of learning and memory. *Commun Biol* **5**, 1148, doi:10.1038/s42003-022-04116-y (2022).

37 Edgar, N. & Sibille, E. A putative functional role for oligodendrocytes in mood regulation. *Transl Psychiatry* **2**, e109, doi:10.1038/tp.2012.34 (2012).

Figure 1 | **Oligodendrocyte deletion by oligodendrocyte-specific AAVs reduces the synchrony of PC population activity during mouse cerebellar development.**

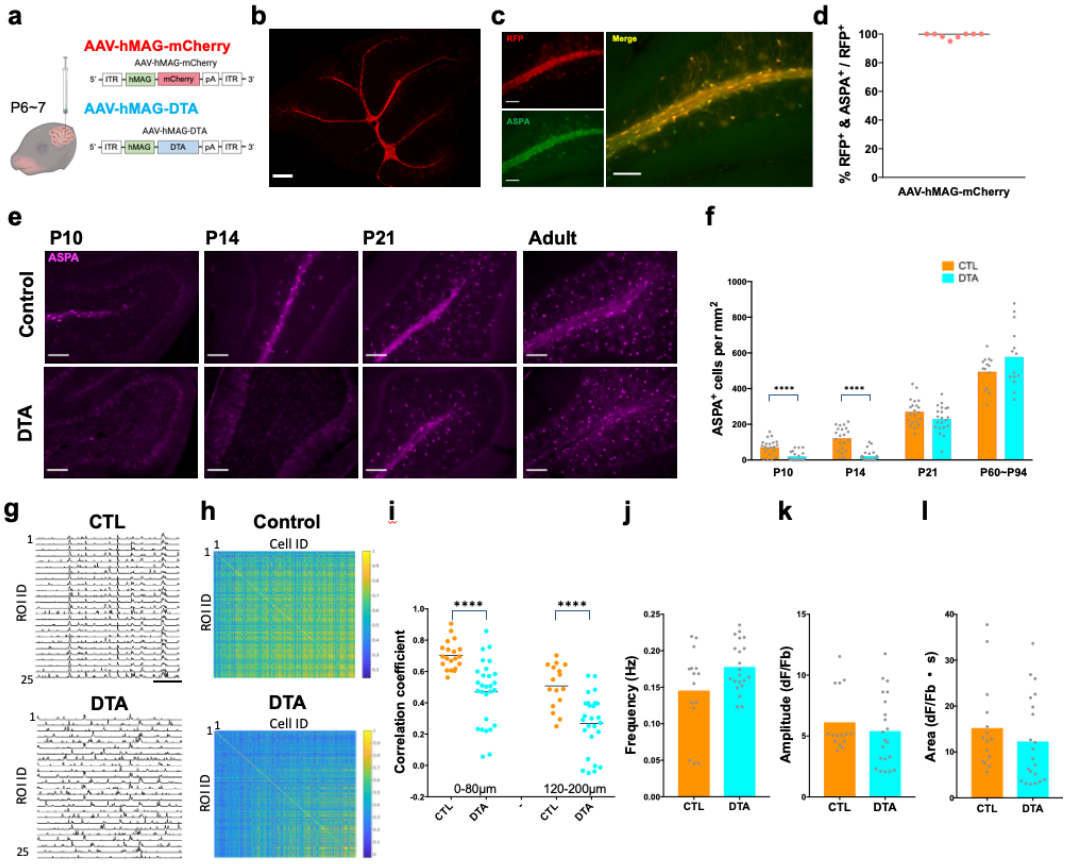

a, Diagram illustrating the injection of AAV-hMAG-mCherry and AAV-hMAG-DTA into the mouse cerebellum at early postnatal days (P6-7). **b**, Fluorescence microscopy image showing mCherry expression (red) in the section of cerebellum at P14 following AAV-hMAG-mCherry injection at P7. Scale bar, 300 µm. **c**, Specificity of mCherry expression (red) in ASPA-positive oligodendrocytes (green) at P14 by AAV-hMAG-mCherry injection at P7. Scale bar, 100 µm. **d**, Scatter plot graph depicting the percentage of RFP and ASPA double-positive cells among RFP-positive populations (from 2 mice). **e**, Sequential visualization of oligodendrocyte deletion over time, indicated by ASPA staining in cerebellar sections from control (AAV-hMAG-mCherry) and DTA-treated (AAV-hMAG-DTA) mice at P10, P14, P21, and P78. Scale bar, 100 µm. **f**, Quantification of ASPA-positive cell density at each stage (from 3 mice per group per each stage). Bars and dots indicate mean and data from individual fields of view, respectively. **g-i**, Decrease in correlation coefficients (CCs) indicating reduced synchrony of spontaneous activities among PC population at P13-15 following DTA-mediated

oligodendrocyte ablation. **g**, Representative time-course of spontaneous calcium transients by extracting relative fluorescence changes by in vivo calcium imaging captured from 25 regions of interest (ROIs) in the cerebellum of control and DTA-expressing mice at P14. Scale bar = 20 s. Y-axis is $\Delta F/F0 = (F - F0)/(F0)$. **h**, Correlation coefficient matrices for spontaneous calcium transient activity across multiple ROIs in CTL (upper panel) and DTA (lower panel) mice, with the color scale indicating the strength of the correlation between pairs of ROIs. **i**, Scatter plot graph of CCs for ROI pairs, categorized by separation distances of 0–80 mm and 120–200 mm (analyzed from four mice per group). Lines and plots indicate mean and data from individual separation distances, respectively. **j-l**, Quantification of the frequency, amplitude, and integrated area of calcium transients in control (AAV-hMAG-mCherry) and DTA-treated (AAV-hMAG-DTA) mice at P13-15 (data from four mice per group). Bars and dots indicate mean and data from individual ROIs, respectively. **** $p < 0.0001$ (Mann-Whitney U test).

Figure 2 | **Oligodendrocyte deletion impairs synapse elimination.**

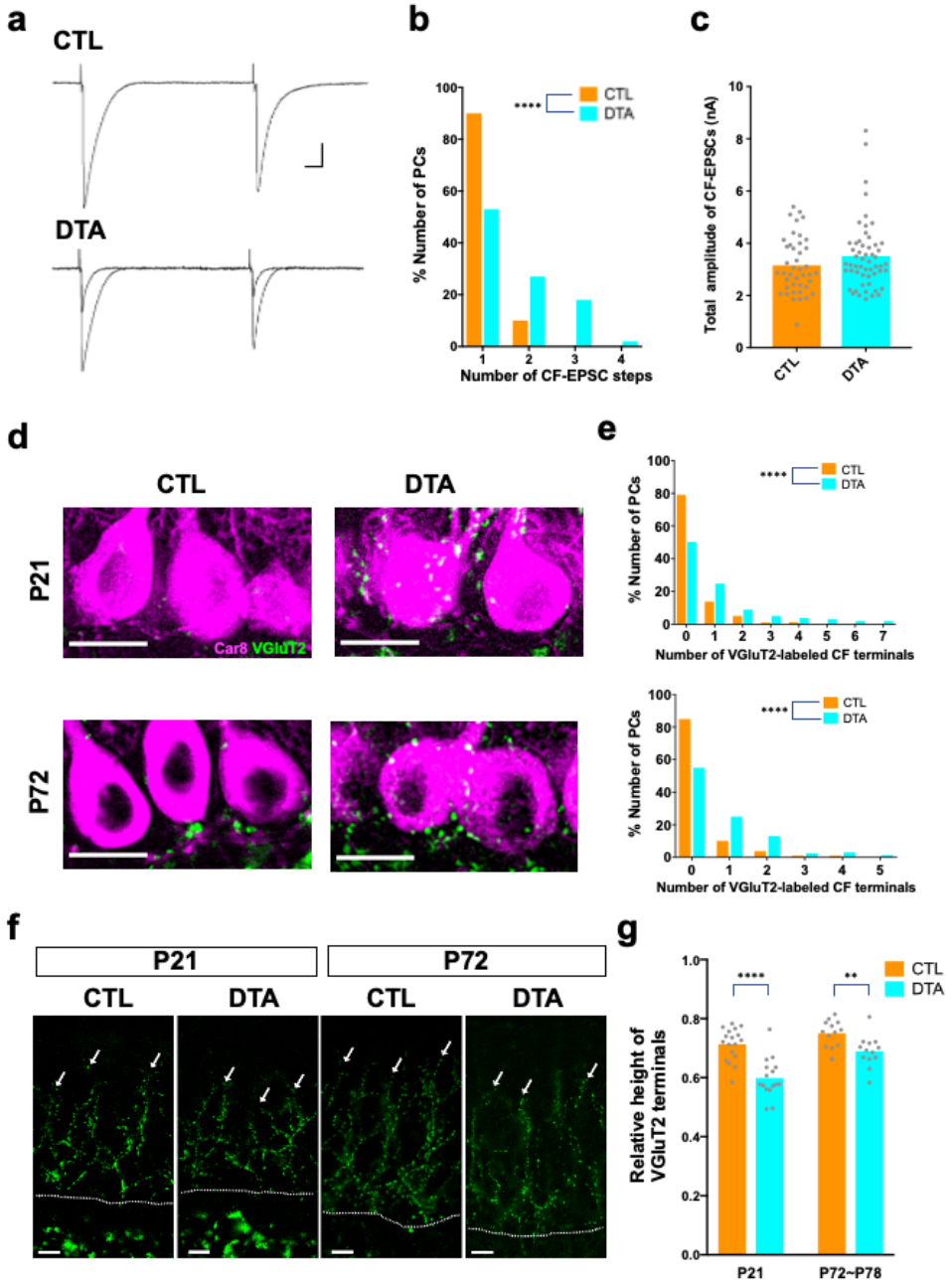

a, Representative traces of CF-EPSCs in PCs from control (CTL) and AAV-hMAG-DTA-injected (DTA) mice at P23. Scale bar, 0.5 nA, 10 ms. **b**, Frequency distributions of the number of CFs innervating each PC during P23 to P47 for control (orange columns, n = 58 cells, 7 mice) and AAV-hMAG-DTA-injected (cyan, n = 66 cells, 9 mice) mice. **c**, Average total amplitude of CF-EPSCs (summation of all CF-EPSC in each PC) for control

(orange columns) and AAV-hMAG-DTA-injected mice (cyan), with individual data points (from each cell) overlaid on the bars. **d**, Fluorescence microscopy images showing PCs labeled with Car8 (magenta) and climbing fiber terminals with vesicular glutamate transporter type 2 (VGluT2, green) in control and AAV-hMAG-DTA-injected mice at P21 and P72. Scale bars: 20 µm. **e,** Frequency distributions of the number of perisomatic CF terminals on PCs for control (orange, n = 253 cells, 3 mice at P12; n = 159 cells, 3 mice at P72-P76) and AAV-hMAG-DTA-injected mice (cyan, n = 157 cells, 3 mice at P12; n = 160 cells, 3 mice at P72-P76). **f**, Immunofluorescence images showing VGluT2 (green) in control and AAV-hMAG-DTA-injected mice at P21 and P72, highlighting the top dots of VGluT2 in the molecular layer (arrows) and the demarcation between dendrites and soma of each PC (dotted line). Scale bars: 20 µm. **g**, Bar graph summarizing the relative positioning of CF terminals to the molecular layer thickness in control versus AAV-hMAG-DTA-injected mice at P21 and P72-P82 (n = 13-18 measurements per group, from 3 mice each). Statistical significance denoted as **$p < 0.01$ and ****$p < 0.0001$, according to Mann-Whitney U tests.

Figure 3 | **Reduced neural synchrony impairs synapse elimination.**

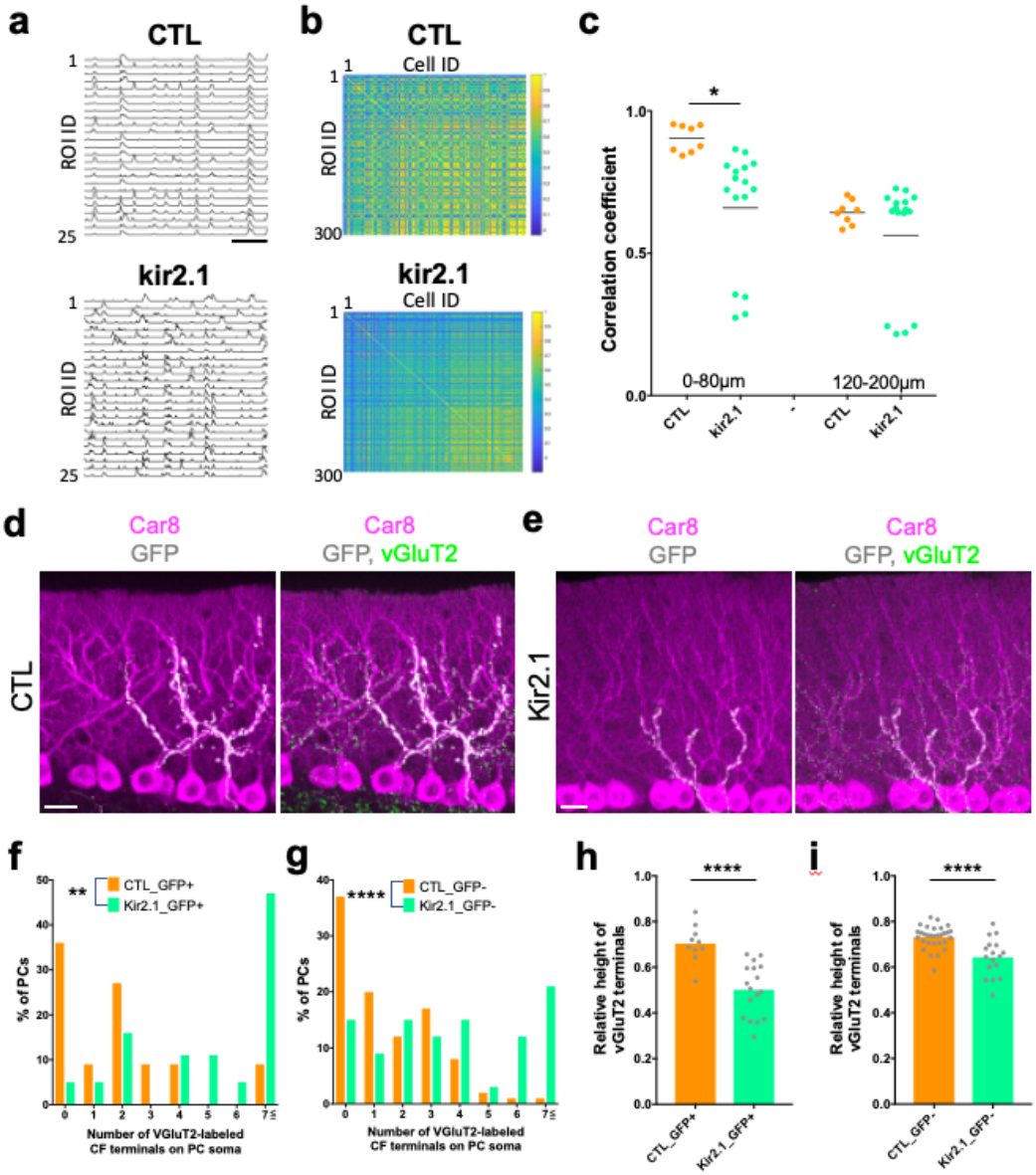

a, Representative time-course of spontaneous calcium transients from regions of interest (ROIs) in the mouse cerebellum at P13 showing spontaneous PC activity in control mice (CTL, top) and mice expressing Kir2.1 in a subset of CFs (kir2.1, bottom). Scale bar, 20 s. Y-axis is ΔF/F0 = (F - F0)/(F0). **b,** Correlation matrices for spontaneous PC activity between ROIs in control (top) and kir2.1-expressing (bottom) mice. The color scale indicates correlation strength. **c,** Scatter plot comparing correlation coefficients for ROI pairs within 0-80μm and 120-200μm separation distance ranges in CTL (orange) and kir2.1-expressing (cyan) mice at P13-15, with lines representing average values. **d-e,** Fluorescence images of PCs labeled with Car8 (magenta)

and GFP-labeled CFs (white), with and without co-labeling for vesicular glutamate transporter type 2 (vGluT2, green), in control (CTL, d) and kir2.1-expressing (Kir2.1, e) mice. Scale bar: 20μm. **f-g,** Frequency histograms showing the distribution of PCs based on the count of vGluT2-labeled CF terminals on the PC soma with GFP-positive (GFP+, **f**) and GFP-negative (GFP-, **g**) CFs within CTL (orange) and kir2.1-expressing (green) mice. **h-i,** Bar graphs representing the mean of the relative height of CF terminals to the molecular layer on PC dendrites with GFP-positive (h) and GFP-negative (i) CFs from CTL (orange) and kir2.1-expressing (green) mice, with individual cells shown as dots. Statistical significance is indicated by asterisks (*$p < 0.05$, **$p < 0.01$, **** $p < 0.0001$, Mann-Whitney U tests).

Figure 4 | **Diminished synchrony of PC population activity leads to behavioral abnormalities.**

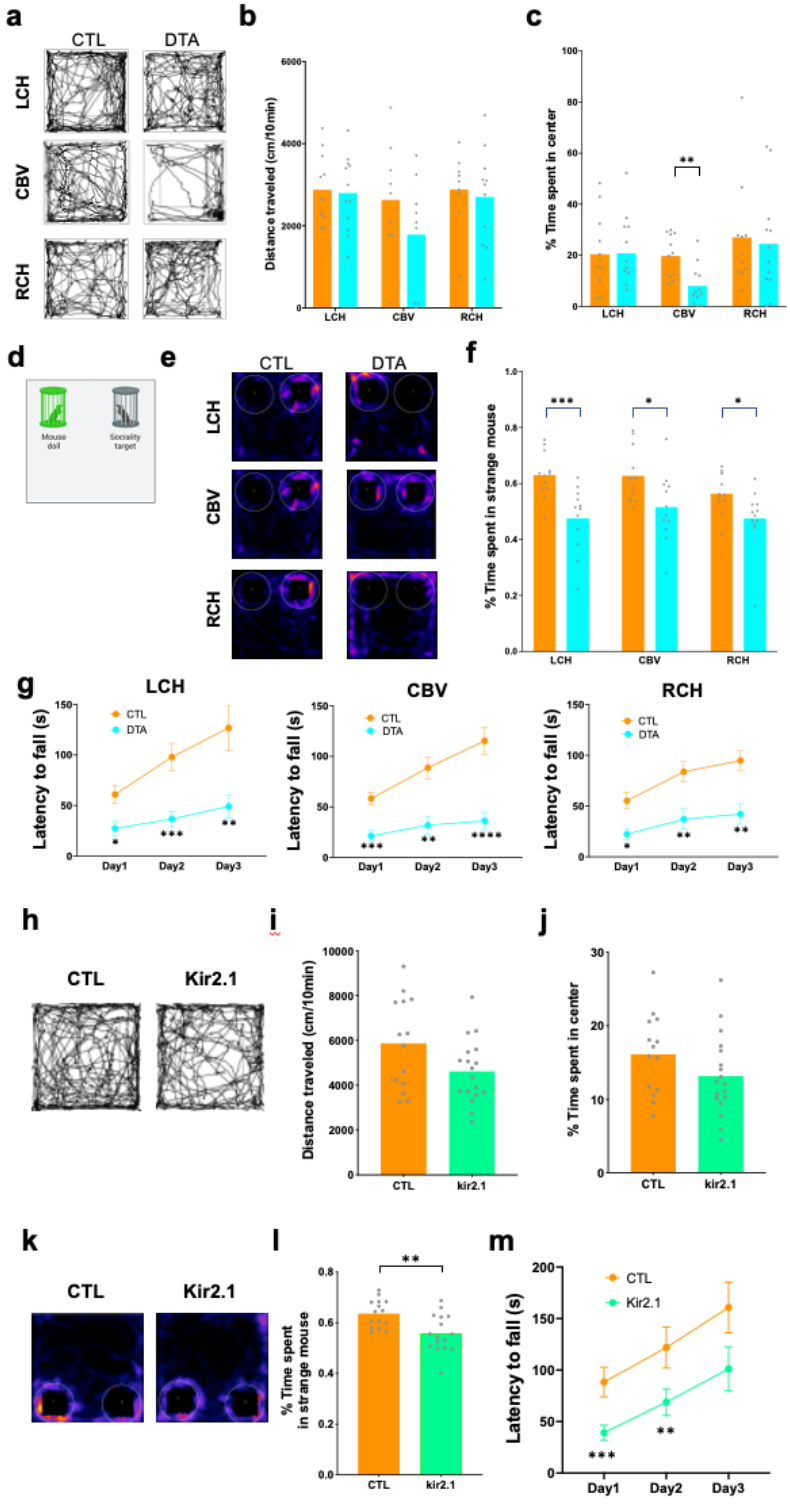

a-c, Assessment of exploratory behavior and locomotor activity in control (CTL, orange) and DTA-injected (DTA, cyan) mice in a novel environment, with trajectories of mouse exploratory behavior (**a**), distance traveled (**b**), and time spent in center (**c**) for mice with the injection of AAVs into distinct compartments (left, center, right) of the cerebellum (LCH, CBV, RCH). Bars and dots indicate mean and data from individual mice, respectively. **d-f,** Representative images and quantitative analysis of sociality in CTL and DTA mice with the injection of AAVs into distinct compartments (LCH, CBV, RCH). Diagram in (**d**) shows the method of sociality test; (**e**) displays the heatmap of mouse exploratory behavior, and (**f**) shows the mean percentage of time spent around strange mouse with data points representing individual mice. **g,** Mena latency to fall in the rotarod test over a three-day period for CTL and DTA mice, with separate graphs for mice with the injection of AAVs into distinct compartments (LCH, CBV, RCH). Error bars indicate SEM. **h-j,** Analysis of exploratory behavior and locomotor activity in CTL (orange) and Kir2.1-expressing (green) mice with distance traveled (**h, i**) and percentage of time spent in the center (**j**) in an open-field test. **k-m,** Representative images and quantitative analysis of sociality in CTL and Kir2.1-expressing mice. (**k**) displays the heatmap of mouse exploratory behavior, and (**l**) shows the percentage of time spent around strange mouse. **m**, Rotarod test. The line graph shows the mean latency to fall across three days for CTL and Kir2.1-expressing mice. Error bars indicate SEM. Statistical significance is indicated by asterisks (*$p < 0.05$, **$p < 0.01$, *** $p < 0.001$, **** $p < 0.0001$, Mann-Whitney U tests).

Materials & Methods

Animals

This study was conducted under the recommendations of the Regulations for Animal Experiments and Related Activities at Tokyo Medical and Dental University. All animal experiment was approved by the Committees on Gene Recombination Experiments and Animal Experiments of Tokyo Medical and Dental University. All animals were group housed and maintained on a 12hr:12hr light dark cycle. All efforts were made to reduce the number of animals used and to minimize the suffering and pain of animals. WT mice (C57BL6N, 6 days -16 weeks, Sankyo labo service) were used in this study.

Plasmids.

The human MAG gene promoter sequences were amplified by PCR from human genomic DNA using primer pairs (Table. 1) and inserted into sites of hSyn promoter in AAV-U6-sgRNA-hSyn-mCherry (a gift from Alex Hewitt, Addgene plasmid # 87916) (AAV-hMAG-mcherry). hSyn promoter was removed by ApaI and BaMH1. The promoter was cloned using the Gibson Cloning Assembly Kit (New England BioLabs) following standard procedures. For AAV-hMAG-DTA, we amplified the DTA coding sequence from the pAAV-mCherry-flex-dtA (a gift from Naoshige Uchida, Addgene plasmid # 58536) using primer pairs (Table. 1) and cloned it into AAV-MAG-mcherry. The sequences of jGCaMP7f gene and jGCaMP7s were amplified by PCR from pGP-AAV-syn-jGCaMP7f-WPRE and pGP-AAV-syn-jGCaMP7s-WPRE (a gift from Douglas Kim & GENIE Project, Addgene plasmid #104488 and #104487) and inserted into sites of GFP in pAAV/L7-6-GFP-WPRE (a gift from Hirokazu Hirai, Addgene plasmid # 126462) (pAAV-L7-6-jGCaMP7f and pAAV-L7-6-jGCaMP7s) and into sites of GFP in pAAV-TRE-EGFP (a gift from Hyungbae Kwon, Addgene plasmid # 89875) (pAAV-TRE-jGCaMP7f and pAAV-TRe-jGCaMP7s). For AAV-TRE-Kir2.1-T2A-GFP, we amplified the sequences of Kir2.1-T2A-GFP from the pAAV hSyn FLEx-loxp Kir2.1-2A-GFP (a gift from Kevin Beier & Robert Malenka, Addgene plasmid # 161574), and cloned it into sites of GFP in pAAV-TRE-EGFP. For AAV-TRE-jGCaMP7f-T2A-Kir2.1, we amplified the sequences of jGCaMP7f and Kir2.1 from the pGP-AAV-syn-jGCaMP7f-WPRE and pAAV hSyn FLEx-loxp Kir2.1-2A-GFP, and cloned it into sites of GFP in pAAV-TRE-EGFP.

AAV packaging and injection.

The AAVs were produced using standard production methods. HEK293 cells were transfected with by Polyethylenimine. AAV9, PHPeB (38) and Olig001 (39) were used. Virus was collected after 120 h from both cell lysates and media. Purification Kit (Takara) was used for viral particle purification. All batches produced were in the range 10^{10} to 10^{11} viral genomes per milliliter. The procedure for viral vector injection has been modified from the previous lentivirus protocol(16). 1-1.5 µL of viral solution were injected into the cerebellum of C57BL/6N mice at 100 nl / min.

Immunohistochemistry.

Mice were perfused with 4% paraformaldehyde in 0.1 M phosphate buffer, and processed for parasagittal microslicer sections (100 µm in thickness). After permeabilization and blockade of nonspecific binding, the following antibodies were applied for 2 days at 4 ^{o}C: an antibody against Car8 (Car8-GP-Af500 or Car8-Go-Af780, diluted 1:300, Nittobo Medical) to visualize PCs; an antibody against S100b (S100b-GP-Af630, 1:300, Nittobo Medical); an antibody against Iba (Wako 019-19741, 1:1000), an antibody against RFP (390004, 1:1000, Synaptic Systems or PM005, 1:500, MBL), an antibody against MBP (NBP2-50035, 1:1000, Novus), an antibody against ASPA (ABN16986, 1:1000, Merck), an antibody against vGluT2 (MSFR106290, 1:300, Nittobo Medical), and/or an antibody against GFP (#06083-05, 1:1000, Nacalai Tesque). After incubation with secondary antibodies (an anti-rat Alexa Fluor 488, an anti-guinea pig Cy3, an anti-goat Alexa Fluor 488, an anti-goat Alexa Fluor 647, an anti-mouse Cy5, an anti-rabbit Cy3, an anti-rabbit Alexa Fluor 488), the immunolabeled sections were washed and then examined under a fluorescent microscope (BZ-X700 or BZ-X800, Keyence).

In vivo calcium imaging.

Animals were put on a warm blanket and anesthetized with a mixture of midazolam (4 mg/kg body weight (BW)), butorphanol (5 mg/kg BW), and medetomidine (0.3 mg/kg BW). The depth of anesthesia was constantly monitored by observing pinch-induced forelimb withdrawal reflex. The skin and muscles over the skull were removed and a

metal plate was fixed with dental acrylic cement over the lobule 5-7 of the cerebellar vermis. A craniotomy of 3 mm diameter was made and the dura mater was carefully removed. A sterile circular 3mm diameter glass coverslip (#CS01078 3mm diameter, Matsunami) was put directly on the dura mater and was secured in place with surgical adhesive (Alon-Alpha A, Sankyo). A custom-made metal headplate with a 5 mm circular imaging well was fixed to the skull over the cranial window with dental cement (Super-Bond, Sun-medical, Japan). The head of the mouse was immobilized by attaching the head plate to a custom-made stage. We then administered atipamezole (0.3mg/kg, anti-sedan) (100 μg/g of body weight, intraperitoneal injection) for anesthesia reversal. After a 10 - 15 minutes waiting period, in vivo calcium imaging was performed using an Olympus MVX10 fluorescence microscope or a two-photon microscope (Nikon, AX R MP) equipped with a ×16 objective lens (Nikon, CFI75 LWD 16X W) and an ultrafast laser (Axon 920-2 TPC). During the recordings, the animals were lied on a warm blanket to keep the body temperature at 37°C. Laser power for the two-photon microscope was maintained <20 mW at the sample. Images were obtained in a 2D plane (2048 x 2048 pixels) using Andor SOLIS software (Oxford Instruments, frame rate 5 Hz) or in a 2D plane (512 × 512 pixels) using Nikon NIS-Elements software (frame rate, 1 Hz) for the two photon microscope. Data were saved as TIFF files.

We resized raw calcium imaging videos (TIFF format) to a resolution of 512 x 512 pixels with a 8-bit depth using ImageJ (JAVA-based processing program, USA). We cropped out the unwanted areas. Regions of interest (ROIs) corresponding to the active PC dendrites were detected using the Suite2p software (Marius Pachitariu, GitHub). This software executed a two-dimensional phase-correlation-based non-rigid image registration in the XY plane, extracted the ROIs considered as PC dendrites, and calculated the fluorescence intensity changes in each ROI. We exported these data as MAT files. The MAT files were imported into MATLAB R2023b (MathWorks, USA) for further analysis using custom-made MATLAB routines. The fluorescence intensity (F) was converted to ΔF/F0 wave, expressed as ΔF/F0 = (F - F0)/(F0), where F0 is the baseline fluorescence in the absence of calcium transients. F0 was defined as follows. First, we calculated a threshold as mean + 1 SD of the F wave of each ROI, and then the F wave below the threshold was averaged to obtain F0. Parameters such as amplitude,

frequency, half-width, and area of each calcium transient were quantified by the custom-made MATLAB routines. The correlation coefficient among all ROI pairs was calculated as previously described (40). The resulting correlation matrix captured relationships among all ROI pairs in the dataset.

Electrophysiology

Control and UNO mice were anesthetized with carbon dioxide and sacrificed by decapitation. The ages of mice were > P21 for climbing fiber-mediated EPSCs (CF-EPSCs). Parasagittal cerebellar slices (with 250 μm thickness) were prepared as described previously (41). The slices were then bathed in a reservoir chamber in an external solution composed of 125 mM NaCl, 2.5 mM KCl, 2 mM $CaCl_2$, 1 mM $MgSO_4$, 1.25 mM NaH_2PO_4, 26 mM $NaHCO_3$, and 20 mM glucose, which was bubbled with 95% O_2 and 5% CO_2 for further 30 min before being transferred to the recording chamber on the stage of an Olympus BX51WI microscope. The chamber was perfused continuously with oxygenated external solution. Picrotoxin (Tocris; 0.1 mM) was added to the bath solution to block $GABA_A$ receptor-mediated inhibitory synaptic transmission. The temperature of the chamber in all experiments was held at 32°C. Patch pipettes were filled with an intracellular solution composed of 60 mM CsCl, 10 mM Cs D-gluconate, 20 mM TEA-Cl, 20 mM BAPTA, 4 mM $MgCl_2$, 4 mM ATP, and 30 mM HEPES (pH 7.3, adjusted with CsOH) for recording CF-EPSCs. The resistance of patch pipette was usually between 1.5–2.5 MΩ and the pipette access resistance was compensated by 70%. CF-EPSCs were elicited at a holding potential of -10 mV or -70 mV by electrical pulse stimuli (duration, 0.1 ms) at 0.2 Hz applied to the granule cell layer 20–100 μm from the targeted PC soma. To search all the CFs innervating the PC under recording, stimulation was applied at up to 10 different locations and the stimulus current intensity was gradually increased from 0 to 30 μA at each location. PFs were stimulated in the molecular layer at the position where a maximum response was elicited with the stimulus current of 5 μA. Then, the stimulus intensity was decreased gradually from 4.5 μA to 0 μA to obtain input-output relations. The recording of mIPSCs was started 4 minutes after the rapture of PC mem- brane.

Behaviors.

Male mice from 2 to 3 months of age 6-7 days after AAV injection were used for behavioral tests. Before the experiments, the mice were habituated in the testing areas for at least 30 min. Mice behavior was recorded through the video camera set in the experimental room. The open field test was performed in a 50 cm x 50 cm x 40 cm (W x D x H) open field box for 10 min. Total distance mice traveled and the time in the center and peripheral regions were automatically analyzed by the ImageJ software (MouBeAT) (42).

The sociality test was performed in the open field apparatus (50 x 50 x 40 cm, W x D x H). The test consisted of a 10-min habituation session and a 10-min test session. In the habituation session, mice were allowed to explore the open field freely. In the test session, two quadrangular cages with slits (8 cm x 8 cm, 18 cm high) were placed in two adjacent corners. One cage contained a novel mouse (8-week-old male C57BL6N) and the other was a mouse doll, and a test mouse was first placed in the outer regions of open field arena at the longest distance from these cages. The times spent around the two cages areas (12 cm in diameter) were analyzed automatically with the ImageJ software (MouBeAT). Social preference was assessed by the following equation: Sociality index = $(T_{mouse})/(T_{doll})$ where T_{mouse} and T_{doll} are the staying time around the mouse cage and that around the doll cage, respectively.

To assess motor coordination and motor learning, mice were subjected to a rotarod test. Mice were placed on a resting state rotarod (model LE8205, Panlab) for three consecutive days with two trials per day spaced 10 min apart (30 min and 40 min after CNO injection). For each trial, the rotarod was accelerated linearly from 4 rpm to 40 rpm over 300 s. Latency to fall from the start of rotation was measured.

Statistical analysis

All data are presented as mean ± SEM. Statistical significance was assessed by Mann-Whitney U test for the comparison of two independent samples. To compare the two different categorical independent samples on one dependent variable, Two-way ANOVA with post-hoc test (Bonferroni correction) was used as indicated in the text. Statistical analysis was conducted with GraphPad Prism program. Differences between

groups were judged to be significant when p values were smaller than 0.05. *, **, ***, **** and ns represents $p < 0.05$, $p < 0.01$, $p < 0.001$, $p < 0.0001$ and not significant, respectively.

1. J. B. Ackman, M. C. Crair, Role of emergent neural activity in visual map development. *Current opinion in neurobiology* **24**, 166-175 (2014).
2. L. A. Kirkby, G. S. Sack, A. Firl, M. B. Feller, A role for correlated spontaneous activity in the assembly of neural circuits. *Neuron* **80**, 1129-1144 (2013).
3. S. Fujimoto *et al.*, Activity-dependent local protection and lateral inhibition control synaptic competition in developing mitral cells in mice. *Dev Cell* **58**, 1221-1236 e1227 (2023).
4. T. A. Babola *et al.*, Homeostatic Control of Spontaneous Activity in the Developing Auditory System. *Neuron* **99**, 511-524 e515 (2018).
5. H. Adelsberger, O. Garaschuk, A. Konnerth, Cortical calcium waves in resting newborn mice. *Nat Neurosci* **8**, 988-990 (2005).
6. T. Murakami, T. Matsui, M. Uemura, K. Ohki, Modular strategy for development of the hierarchical visual network in mice. *Nature* **608**, 578-585 (2022).
7. J. M. Good *et al.*, Maturation of Cerebellar Purkinje Cell Population Activity during Postnatal Refinement of Climbing Fiber Network. *Cell Rep* **21**, 2066-2073 (2017).
8. H. Mizuno *et al.*, Patchwork-Type Spontaneous Activity in Neonatal Barrel Cortex Layer 4 Transmitted via Thalamocortical Projections. *Cell Rep* **22**, 123-135 (2018).
9. D. Kato *et al.*, Motor learning requires myelination to reduce asynchrony and spontaneity in neural activity. *Glia* **68**, 193-210 (2020).
10. S. Pajevic, P. J. Basser, R. D. Fields, Role of myelin plasticity in oscillations and synchrony of neuronal activity. *Neuroscience* **276**, 135-147 (2014).
11. S. Pajevic, D. Plenz, P. J. Basser, R. D. Fields, Oligodendrocyte-mediated myelin plasticity and its role in neural synchronization. *Elife* **12** (2023).
12. M. Kano, T. Watanabe, N. Uesaka, M. Watanabe, Multiple Phases of Climbing Fiber Synapse Elimination in the Developing Cerebellum. *Cerebellum* **17**, 722-734 (2018).

13. M. Kano, T. Watanabe, Developmental synapse remodeling in the cerebellum and visual thalamus. *F1000Res* **8** (2019).
14. P. Penzes, M. E. Cahill, K. A. Jones, J. E. VanLeeuwen, K. M. Woolfrey, Dendritic spine pathology in neuropsychiatric disorders. *Nat Neurosci* **14**, 285-293 (2011).
15. M. Kano *et al.*, Impaired synapse elimination during cerebellar development in PKCγ mutant mice. *Cell* **83**, 1223-1231 (1995).
16. N. Uesaka *et al.*, Retrograde semaphorin signaling regulates synapse elimination in the developing mouse brain. *Science* **344**, 1020-1023 (2014).
17. K. Hashimoto *et al.*, Roles of glutamate receptor δ2 subunit (GluRδ2) and metabotropic glutamate receptor subtype 1 (mGluR1) in climbing fiber synapse elimination during postnatal cerebellar development. *J Neurosci* **21**, 9701-9712 (2001).
18. H. Kurihara *et al.*, Impaired parallel fiber-->Purkinje cell synapse stabilization during cerebellar development of mutant mice lacking the glutamate receptor δ2 subunit. *J Neurosci* **17**, 9613-9623 (1997).
19. H. Nakayama *et al.*, GABAergic inhibition regulates developmental synapse elimination in the cerebellum. *Neuron* **74**, 384-396 (2012).
20. T. Miyazaki *et al.*, Glutamate transporter GLAST controls synaptic wrapping by Bergmann glia and ensures proper wiring of Purkinje cells. *Proc Natl Acad Sci U S A* **114**, 7438-7443 (2017).
21. H. Nakayama *et al.*, Microglia permit climbing fiber elimination by promoting GABAergic inhibition in the developing cerebellum. *Nat Commun* **9**, 2830 (2018).
22. L. W. Bosman, H. Takechi, J. Hartmann, J. Eilers, A. Konnerth, Homosynaptic long-term synaptic potentiation of the "winner" climbing fiber synapse in developing Purkinje cells. *J Neurosci* **28**, 798-807 (2008).
23. Y. Kawamura *et al.*, Spike timing-dependent selective strengthening of single climbing fibre inputs to Purkinje cells during cerebellar development. *Nat Commun* **4**, 2732 (2013).
24. K. Hashimoto *et al.*, Postsynaptic P/Q-type Ca2+ channel in Purkinje cell mediates synaptic competition and elimination in developing cerebellum. *Proc Natl Acad Sci U S A* **108**, 9987-9992 (2011).
25. K. Dorgans, D. Guo, K. Kurima, J. Wickens, M. Y. Uusisaari, Designing AAV Vectors for Monitoring the Subtle Calcium Fluctuations of Inferior Olive Network in vivo. *Front Cell Neurosci* **16**, 825056 (2022).

26. X. Guell, J. D. Schmahmann, J. Gabrieli, S. S. Ghosh, Functional gradients of the cerebellum. *Elife* **7** (2018).
27. E. Manni, L. Petrosini, A century of cerebellar somatotopy: a debated representation. *Nature reviews. Neuroscience* **5**, 241-249 (2004).
28. G. Bonetto, D. Belin, R. T. Karadottir, Myelin: A gatekeeper of activity-dependent circuit plasticity? *Science* **374**, eaba6905 (2021).
29. M. Jang, E. Gould, J. Xu, E. J. Kim, J. H. Kim, Oligodendrocytes regulate presynaptic properties and neurotransmission through BDNF signaling in the mouse brainstem. *Elife* **8** (2019).
30. R. D. Fields, A new mechanism of nervous system plasticity: activity-dependent myelination. *Nature reviews. Neuroscience* **16**, 756-767 (2015).
31. Y. Liu *et al.*, Interactions of glial cells with neuronal synapses, from astrocytes to microglia and oligodendrocyte lineage cells. *Glia* **71**, 1383-1401 (2023).
32. D. K. Wilton, L. Dissing-Olesen, B. Stevens, Neuron-Glia Signaling in Synapse Elimination. *Annu Rev Neurosci* **42**, 107-127 (2019).
33. Y. S. S. Auguste *et al.*, Oligodendrocyte precursor cells engulf synapses during circuit remodeling in mice. *Nat Neurosci* **25**, 1273-1278 (2022).
34. Y. Yamazaki *et al.*, Region- and Cell Type-Specific Facilitation of Synaptic Function at Destination Synapses Induced by Oligodendrocyte Depolarization. *J Neurosci* **39**, 4036-4050 (2019).
35. O. de Faria, Jr. *et al.*, Periods of synchronized myelin changes shape brain function and plasticity. *Nat Neurosci* **24**, 1508-1521 (2021).
36. M. Munyeshyaka, R. D. Fields, Oligodendroglia are emerging players in several forms of learning and memory. *Commun Biol* **5**, 1148 (2022).
37. N. Edgar, E. Sibille, A putative functional role for oligodendrocytes in mood regulation. *Transl Psychiatry* **2**, e109 (2012).
38. K. Y. Chan *et al.*, Engineered AAVs for efficient noninvasive gene delivery to the central and peripheral nervous systems. *Nat Neurosci* **20**, 1172-1179 (2017).
39. S. K. Powell *et al.*, Characterization of a novel adeno-associated viral vector with preferential oligodendrocyte tropism. *Gene Ther* **23**, 807-814 (2016).
40. S. Tsutsumi *et al.*, Structure-function relationships between aldolase C/zebrin II expression and complex spike synchrony in the cerebellum. *J. Neurosci.* **35**, 843-852 (2015).
41. A. Aiba *et al.*, Deficient cerebellar long-term depression and impaired motor learning in mGluR1 mutant mice. *Cell* **79**, 377-388 (1994).

42. E. Bello-Arroyo *et al.*, MouBeAT: A New and Open Toolbox for Guided Analysis of Behavioral Tests in Mice. *Front Behav Neurosci* **12**, 201 (2018).